liquid nitrogen in the operating room and stored at −80°C until use for the detection of viral genomes. Twenty American patients with ischemic cardiomyopathy who received heart transplants at Henry Ford Hospital and 28 Japanese patients who underwent aneurysmectomy or Dor's operation at Osaka Medical College Hospital or Shonan Kamakura General Hospital were also included.

Detection of viral genome: In situ hybridization studies have shown uneven distributions of enteroviruses in the myocardium of patients with myocarditis and IDC.[8] Thus, we analyzed 5 different regions of the patient myocardium resected at heart transplantation or PLV to determine the true frequency of viral infection in hearts with IDC. Total RNA and genomic and viral deoxyribonucleic acid (DNA) were extracted from 20 mg of myocardial tissue obtained from each region of patient specimens using ABI-340A Nucleic Acid Extractor (PE-Applied Biosystems, Foster City, California), according to the standard program supplied by the manufacturer. Ten micrograms of extracted total RNA were used for each viral first complementary DNA (cDNA) synthesis.[19–21] Strand-specific enteroviral RNA detection was performed to differentiate between active viral replication and latent viral persistence in hearts with IDC.[19] First-strand cDNA synthesis was primed with reverse polymerase chain reaction (PCR) primer for plus-strand enteroviral RNA detection and forward PCR primer for the detection of minus-strand enteroviral RNA. The reverse transcription mixture was boiled for 30 minutes to terminate the enzyme activity of the reverse transcriptase. Then, PCR amplification, followed by Southern blot hybridization, analysis was performed. A portion of the VP1 region of the enteroviral genome was used for the identification of enteroviruses detected in hearts with IDC.[22] PCR-amplified products were gel isolated and purified using the Concert Gel Extraction Systems (Gibco-GRL, Rockville, Maryland).[11] The nucleotide sequences were determined in each direction using an automated DNA sequencer with fluorescent dideoxy-chain terminators (PE-Applied Biosystems). Conventional reverse transcription–PCR (RT-PCR) was used for the genomic detection of mumps virus[20] and influenza A and B viruses.[21] Ten micrograms of extracted DNA were used for PCR detection of each genomic nucleic acid of adenovirus,[15] parvovirus,[16] herpes simplex 1 and 2 viruses, varicella-zoster virus,[23] and Epstein-Barr virus.[24] Independent RT-PCR and PCR were carried out on each sample with β-actin primers to confirm the use of sufficient amount of extracted RNA and DNA.[25] Several negative controls were included in each reaction. The frequency of each viral genome in American patients with IDC was compared with that in Japanese patients with IDC. Statistical analysis was performed using Fisher's exact test, and a p value of <0.05 was considered significant.

RESULTS

Patient profile: Thirty American patients with IDC (18 men and 12 women; mean age 46 ± 16 years) and 47 Japanese patients with IDC (34 men and 13 women; mean age 48 ± 14 years) were studied for the presence of viral genomes. All patients had end-stage IDC and were in New York Heart Association functional class III or IV. The durations of illness of American and Japanese patients were 78 ± 30 and 62 ± 41 months, respectively. All patients had an increased left ventricular end-diastolic diameter and globally impaired left ventricular function as assessed by echocardiography. No patients had evidence of hypertension, valvular heart disease, drug or alcohol abuse, or systemic disorders. Angiography showed no evidence of coronary artery disease. All specimens had a histologic appearance consistent with the diagnosis of IDC. Left ventricular specimens from 20 American patients with ischemic cardiomyopathy (14 men and 6 women; mean age 58 ± 8 years) and 28 Japanese patients with coronary artery disease (21 men and 7 women; mean age 59 ± 11 years) served as control specimens.

TABLE 1 Detection of Viral Genomes in the Myocardium of Patients With IDC

Virus	American Patients (n = 30)	Japanese Patients (n = 47)
RNA viruses		
Enterovirus		
Coxsackie A virus	0/30 (0%)	0/47 (0%)
Coxsackie B virus	7/30 (23%)	15/47 (32%)
Echovirus	0/30 (0%)	0/47 (0%)
Mumps virus	0/30 (0%)	0/47 (0%)
Influenza A virus	0/30 (0%)	0/47 (0%)
Influenza B virus	0/30 (0%)	0/47 (0%)
DNA viruses		
Adenovirus	0/30 (0%)	0/47 (0%)
Parvovirus	0/30 (0%)	0/47 (0%)
Herpes simplex 1 virus	0/30 (0%)	0/47 (0%)
Herpes simplex 2 virus	0/30 (0%)	0/47 (0%)
Varicella-zoster virus	0/30 (0%)	0/47 (0%)
Epstein-Barr virus	0/30 (0%)	0/47 (0%)

Detection of viral genome: We studied 5 different regions of each resected myocardium, and the same PCR detection results were obtained (Table 1). Strand-specific enteroviral RNA detection was performed to determine viral activity in the myocardium of patients with IDC. During enteroviral replication, the genomic viral plus-strand RNA serves as a template for the transcription of a minus-strand RNA. This minus-strand viral RNA is then used as a template to produce multiple plus-strand viral RNA to be translated into enteroviral proteins and packaged into new virions. Therefore, the detection of minus-strand viral RNA is an indicator of active enteroviral RNA replication.[26] Figure 1 shows a representative Southern blot hybridization analysis of the amplified PCR products. Plus-strand enteroviral RNA was detected in 7 of the 30 American patients (23%) with IDC. Minus-strand viral RNA was demonstrated in 5 of these 7 plus-strand-positive patients (71%). In the Japanese patients with IDC, plus-strand enteroviral RNA was detected in 15 of the 47 patients (32%). Minus-strand viral RNA was present in 12 of these 15 plus-strand-

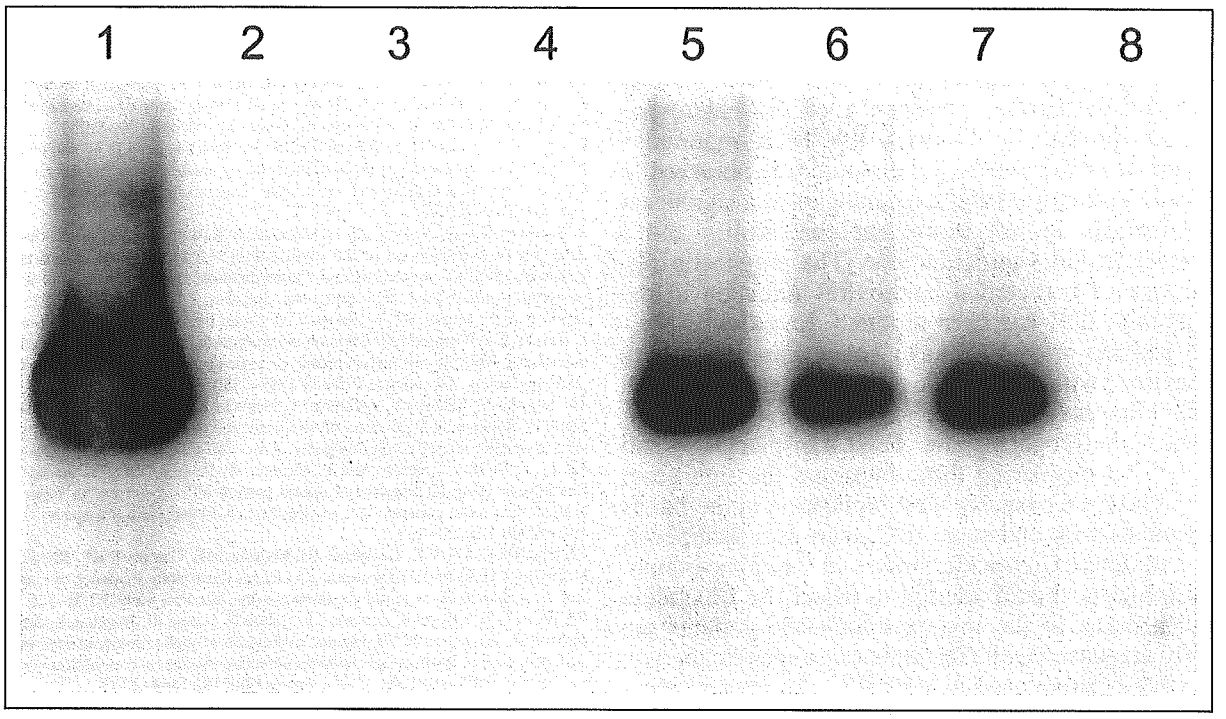

FIGURE 1. Strand-specific enteroviral RNA detection in the myocardium of 3 different patients. Southern blot hybridization analysis of PCR products with enterovirus-specific P^{32}-labeled probe is shown. In *lanes 3, 5, and 7,* RT-PCR was performed with 3′ enteroviral primer for RT. The signals seen in *lanes 5 and 7* correspond to enteroviral plus-strand cDNA. In *lanes 4, 6, and 8,* RT-PCR was carried out with 5′ enteroviral primer for RT. The signal seen in *lane 6* corresponds to enteroviral minus-strand cDNA. In summary, patient A *(lanes 5 and 6)* shows active enteroviral replication (minus-strand detectable). Patient B *(lanes 7 and 8)* shows latent virus persistence (not minus-strand detectable). Patient C *(lanes 3 and 4)* is negative for enteroviral genome. *Lane 1,* positive control of Coxsackie B1 cloned DNA. *Lane 2,* negative control.

positive patients (80%). Nucleotide sequence data were obtained on the 607 base pair PCR products, a part of the VP1 coding region of the enteroviral genome. The sequences from 5 American patients and 7 Japanese patients exhibited significant homology (92.1% to 99.3%) with that of Coxsackie virus B3, strain Nancy. Sequencing of the PCR products from the remaining hearts was incomplete and resembled Coxsackie B viruses. Therefore, active Coxsackie virus RNA replication in the myocardium was present in a significant proportion of virus-positive American and Japanese patients with end-stage IDC. Histology revealed that the presence of severe cell infiltration in 5 of 7 Coxsackie virus positive American patients and in 9 of 15 Coxsackie virus positive Japanese patients. Inflammatory infiltrates appeared to be associated with persistent Coxsackie virus infection. There was no significant difference in Coxsackie viral positivity between American and Japanese patients. Genomic nucleic acid sequences for influenza A and B viruses, mumps virus, adenovirus, parvovirus, herpes simplex 1 and 2 viruses, varicella-zoster virus, and Epstein-Barr virus were not detected in the myocardium of either American or Japanese patients with IDC. No viral genomes were found in the control specimens. All samples had β-actin sequences demonstrated by RT-PCR and PCR, indicating the adequate extraction of RNA and DNA. The PCR results for each virus were negative in all of the negative controls.

DISCUSSION

It has not been possible to consistently identify the underlying mechanisms and to etiologically design specific therapy for patients with IDC. Viral infection and genetic disorders are the best defined and most commonly identified causes of this disease.[1,2] However, the worldwide prevalence of viral infection in hearts with IDC has not been investigated. We evaluated infection with a variety of viruses in the myocardium of American and Japanese patients with end-stage IDC. A significant detection rate of Coxsackie B viruses in the myocardium emphasizes the importance of these viruses as causative agents in American and Japanese patients with IDC. Therefore, Coxsackie B viruses should be studied to determine the mechanism responsible for the progression from acute myocardial infection to dilated cardiomyopathy. The large incidence of Coxsackie virus RNA would be due to the size of the myocardial specimens examined. Therefore, the use of multiple biopsy samples is considered to be necessary to determine the true frequency of viruses in hearts with IDC.

We also demonstrated that Coxsackie viral RNA replicates actively in a significant proportion of virus-positive American and Japanese patients with end-stage IDC. This finding is important in view of the pathogenesis of this disease and the treatment of patients with this disease, because experiments show that restricted Coxsackie viral RNA replication in the

myocardium can impair cardiac contractile function and lead to dilated cardiomyopathy.[14] Recently, very important data from an interferon treatment of patients with the myocardial persistence of the enteroviral genome proved by biopsies has been reported.[27] Clearance of the enteroviral genome was observed in all patients analyzed and are paralleled to a significant improvement in left ventricular contractility and a decrease in left ventricular size. The prognostic significance of myocardial enterovirus infection in patients with IDC has been reported. Enterovirus-positive patients with IDC have an increased mortality compared with enterovirus-negative patients with IDC.[10] Enterovirus persistence in the myocardium influences the prognosis after heart transplantation and PLV.[11,28] Considering these facts and the significant rate of active Coxsackie viral replication in the hearts of patients with end-stage IDC, there is a therapeutic need to detect Coxsackie viruses in the myocardium. Cardiologists should attempt to detect the Coxsackie viral genome in the myocardium when patients are newly diagnosed with IDC and design specific therapy for virus-positive patients with IDC. An improvement in cardiac function should be expected by eliminating viruses from the myocardium. Although not yet available, effective vaccines for groups at risk may be useful for the prevention of cardiovirulent Coxsackie viral infection.

There was no evidence of persistent infection with other viruses, including adenovirus or parvovirus, in the myocardium of either American or Japanese patients with end-stage IDC. However, patients in the earlier stages of the disease should be examined. The persistence of immune response after clearance of the virus cannot be completely ruled out.

In conclusion, active group B Coxsackie virus RNA replication in the myocardium was demonstrated in a significant percentage of American and Japanese patients with end-stage IDC. There was no evidence of persistent infection with other viruses in hearts with IDC. Specific therapy should be designed for Coxsackie virus positive patients with IDC.

1. Martino TA, Liu P, Sole MJ. Viral infection and the pathogenesis of dilated cardiomyopathy. *Circ Res* 1994;74:182–188.
2. Cooper LT, Jr, Gersh BJ. Viral infection, inflammation, and the risk of idiopathic dilated cardiomyopathy: can the fire be extinguished? *Am J Cardiol* 2002;90:751–754.
3. Quigley PJ, Richardson PJ, Meany BT, Olsen EGJ, Monaghan MJ, Jackson G, Jewitt DE. Long-term follow-up of acute myocarditis. Correlation of ventricular function and outcome *Eur Heart J* 1987;8(suppl J):39–42.
4. Kitaura Y. Virological study of idiopathic cardiomyopathy: serological study of virus antibodies and immunofluorescent study of myocardial biopsies. *Jpn Circ J* 1981;45:279–294.
5. Muir P, Nicholson F, Tilzey AJ, Signy M, English TAH, Banatvala JE. Chronic relapsing pericarditis and dilated cardiomyopathy: serological evidence of persistent enterovirus infection. *Lancet* 1989;1:804–807.
6. Morita H. Experimental coxsackie B virus myocarditis in golden hamsters, light and electron microscopy findings in a long-term follow-up study. *Jpn Circ J* 1981;45:713–729.
7. Bowles NE, Archard LC, Olsen EGJ, Richardson PJ. Detection of coxsackie-B-virus-specific RNA sequences in myocardial biopsy samples from patients with myocarditis and dilated cardiomyopathy. *Lancet* 1986;1:1120–1123.
8. Kandolf R, Ameis D, Kirschner P, Canu A, Hofschneider PH. In situ detection of enteroviral genomes in myocardial cells by nucleic acid hybridization: an approach to the diagnosis of viral heart disease. *Proc Natl Acad Sci USA* 1987;84:6272–6276.
9. Koide H, Kitaura Y, Deguchi H, Ukimura A, Kawamura K, Hirai K. Genomic detection of enteroviruses in the myocardium—studies on animal hearts with coxsackievirus B3 myocarditis and endomyocardial biopsies from patients with myocarditis and dilated cardiomyopathy. *Jpn Circ J* 1992;56:1081–1093.
10. Why HJF, Meany BT, Richardson PJ, Olsen EGJ, Bowles NE, Cunningham L, Freeke CA, Archard LC. Clinical and prognostic significance of detection of enteroviral RNA in the myocardium of patients with myocarditis or dilated cardiomyopathy. *Circulation* 1994;89:2582–2589.
11. Fujioka S, Kitaura Y, Ukimura A, Deguchi H, Kawamura K, Isomura T, Suma H, Shimizu A. Evaluation of viral infection in the myocardium of patients with idiopathic dilated cardiomyopathy. *J Am Coll Cardiol* 2000;36:1920–1926.
12. Li Y, Bourlet T, Andreoletti L, Mosnier JF, Peng T, Yang Y, Archard LC, Pozzetto B, Zang H. Enteroviral capsid protein VP1 is present in myocardial tissues from some patients with myocarditis or dilated cardiomyopathy. *Circulation* 2000;101:231–234.
13. Badorff C, Lee GH, Lamphear BJ, Martone ME, Campbell KP, Rhoads RE, Knowlton KU. Enteroviral protease 2A cleaves dystrophin: evidence of cytoskeletal disruption in an acquired cardiomyopathy. *Nat Med* 1999;5:320–326.
14. Wessely R, Klingel K, Santana LF, Dalton N, Hongo M, Jonathan Lederer W, Kandolf R, Knowlton K. Transgenic expression of replication-restricted enteroviral genomes in heart muscle induces defective excitation-contraction coupling and dilated cardiomyopathy. *J Clin Invest* 1998;102:1444–1453.
15. Pauschinger M, Bowles NE, Garcia JF, Kuhl U, Schwimmbeck PL, Schultheiss HP, Towbin JA. Detection of adenoviral genome in the myocardium of adult patients with idiopathic left ventricular dysfunction. *Circulation* 1999;99:1348–1354.
16. Pankuweit S, Moll R, Baandrup U, Portig I, Hufnagel G, Maisch B. Prevalence of the parvovirus B19 genome in endomyocardial biopsy specimens. *Hum Pathol* 2003;34:497–503.
17. Feldman AM, McNamara D. Myocarditis. *N Engl J Med* 2000;343:1388–1398.
18. Richardson P, McKenna W, Bristow M, Maisch B, Mautner B, O'Connel J, Olsen E, Thiene G, Goodwin J, Gyarfas I, et al. Report of the 1995 World Health Organization/International Society and Federation of Cardiology task force on the definition and classification of cardiomyopathies. *Circulation* 1996;93:841–842.
19. Pauschinger M, Doerner A, Kuehl U, Schwimmbeck PL, Poller W, Kandolf R, Schultheiss HP. Enteroviral RNA replication in the myocardium of patients with left ventricular dysfunction and clinically suspected myocarditis. *Circulation* 1999;99:889–895.
20. Boriskin YS, Booth JC, Yamada A. Rapid detection of mumps virus by the polymerase chain reaction. *J Virol Methods* 1993;42:23–32.
21. Zhang W, Evans DH. Detection and identification of human influenza viruses by the polymerase chain reaction. *J Virol Methods* 1991;33:165–189.
22. Casas I, Palacios GF, Trallero G, Cisterna D, Freire MC, Tenorio A. Molecular characterization of human enteroviruses in clinical samples: comparison between VP2, VP1, and RNA polymerase regions using RT nested PCR assays and direct sequencing of products. *J Med Virol* 2001;65:138–148.
23. Beards G, Graham C, Pillay D. Investigation of vesicular rashes for HSV and VZV by PCR. *J Med Virol* 1998;54:155–157.
24. Durmaz R, Aydin A, Koroglu M, Aker H, Ozercan IH, Atik E, Arici S. Detection and genotyping of Epstein-Barr virus by polymerase chain reaction in tissues obtained from cases with Hodgkin's disease in Turkey. *Acta Virol* 1998;42:375–381.
25. Nakajiama-Iijma S, Hamada H, Reddy P, Kakznaga T. Molecular structure of the human cytoplasmic beta-actin gene: interspecies homology of sequences in the introns. *Proc Natl Acad Sci USA* 1985;82:6133–6137.
26. Hohenadl C, Klingel K, Mertsching J, Hofschneider PH, Kandolf R. Strand-specific detection of enteroviral RNA in myocardial tissue by in situ hybridization. *Moll Cell Probes* 1991;5:11–20.
27. Kuhl U, Pauschinger M, Schwimmbeck PL, Seeberg B, Lober C, Noutsias M, Poller W, Kandolf R, Schultheiss HP. Interferon-β treatment eliminates cardiotropic viruses and improves left ventricular function in patients with myocardial persistence of viral genomes and left ventricular dysfunction. *Circulation* 2003;107:2793–2798.
28. Calabrese F, Valente V, Thiene G, Angelini A, Testolin L, Biasolo MA, Soteriou B, Livi U, Palu G. Enteroviral genome in native hearts may influence outcome of patients who undergo cardiac transplantation. *Diagn Mol Pathol* 1999;8:39–46.

Development of biologic coronary artery bypass grafting in a rabbit model: Revival of a classic concept with modern biotechnology

Koji Ueyama, MD[a]
Gao Bing, MD[a]
Yasuhiko Tabata, PhD[b]
Makoto Ozeki, BS[b]
Kazuhiko Doi, MD[a]
Kazunobu Nishimura, MD, PhD[a]
Hisayoshi Suma, MD, PhD[c]
Masashi Komeda, MD, PhD[a]

Objective: We have developed a technique for biologic coronary artery bypass grafting, which is a revival of a classic concept with modern biotechnology.

Methods: Acute myocardial infarction was created by ligating the major branch of the circumflex artery in rabbits. Animals were divided into four groups: a nontreated group (group N), a group in which omentum was used to wrap the infarcted area (group G), a group in which a gelatin hydrogel sheet incorporating 100 μg basic fibroblast growth factor was placed over the infarcted area (group F), and a group in which the infarcted area was similarly treated with basic fibroblast growth factor followed by omental wrapping (group FG). Cardiac function was subsequently assessed by echocardiography. Postmortem angiography through the gastroepiploic artery was done in groups G and FG. Infarct size and arteriolar density were evaluated.

Results: Group FG showed a better fractional area change than did the other groups (group N $P < .001$, group G $P = .002$, group F $P < .001$). Angiography revealed that communication from the gastroepiploic artery to the coronary artery was created through a rich bed of neovascularization in all 7 animals of group FG, whereas poor collaterals were recognized in only 2 of 7 animals in group G. Infarct size was reduced to a greater extent in group FG than in groups F, G, and N (10% $\pm$ 3%, 16% $\pm$ 5%, 19% $\pm$ 7%, 23% $\pm$ 2%, respectively, group F $P = .04$, groups G and N $P < .01$). The number of arterioles 20 to 100 μm in diameter was increased to a greater extent in group FG than in groups F, G, and N (23 $\pm$ 5 arterioles/mm^2, 14 $\pm$ 3 arterioles/mm^2, 10 $\pm$ 1 arterioles/mm^2, 4 $\pm$ 2 arterioles/mm^2, respectively), with the differences being significant.

Conclusions: These results show that bypass from the gastroepiploic artery to coronary arteries can be achieved without surgical anastomosis through slow release of basic fibroblast growth factor in this rabbit acute myocardial infarction model. This new revascularization concept, biologic coronary artery bypass grafting, could be applicable for revascularizing many tiny coronary vessels in patients who are difficult to treat with conventional surgery or catheter intervention.

From the Department of Cardiovascular Surgery, the Graduate School of Medicine,[a] and the Institute for Frontier Medical Sciences,[b] Kyoto University, Kyoto, Japan, and Hayama Heart Center,[c] Kanagawa, Japan.

Read at the Eighty-third Annual Meeting of The American Association for Thoracic Surgery, Boston, Mass, May 4-7, 2003.

Received for publication May 19, 2003; revisions requested Aug 8, 2003; revisions received Aug 11, 2003; accepted for publication Sept 17, 2003.

Address for reprints: Masashi Komeda, MD, PhD, Professor of Cardiovascular Surgery, Graduate School of Medicine, Kyoto University, 54 Shogoin, Sakyo-Ku, Kyoto, Japan PO: 606-8507 (E-mail: masakom@kuhp.kyoto-u.ac.jp).

J Thorac Cardiovasc Surg 2004;127:1608-15

0022-5223/$30.00

doi:10.1016/j.jtcvs.2003.08.043

So-called therapeutic angiogenesis was developed as an alternative to conventional treatments, such as percutaneous coronary intervention and coronary artery bypass grafting (CABG)[1] for advanced coronary artery disease. Many experimental studies have demonstrated excellent results.[2-7] Several clinical studies with therapeutic angiogenesis in patients undergoing CABG have shown improvement in myocardial perfusion according to late nuclear perfusion scans.[8,9]

If the donor coronary artery from which new vessels sprouted by angiogenetic therapy was too far from the ischemic area, however, or if it was too small, diseased, or stenosed, then blood flow through the neovasculature might not be enough to supply the ischemic territory. The efficacy of current forms of therapeutic angiogenesis may not be sufficient for such types of coronary artery territory.

In 1936, O'Shaughnessy[10] introduced a technique, omentopexy, in which the greater omentum was brought through the left diaphragm and wrapped around the ischemic heart. In 1950, Vineberg and Miller introduced internal thoracic artery implantation[11] by modifying the omentopexy technique into a free omental graft operation.[12] Although these classic procedures for treatment of angina pectoris required a long time for graft-coronary communication to mature sufficiently, some experimental studies have demonstrated the connection between omental vessels and the coronary artery by angiography, and some clinical reports have described a good outcome after pedicled or free omental grafting.[3-16]

We previously reported that use of a gelatin sheet incorporating basic fibroblast growth factor (bFGF) can offset sternal ischemia and accelerate sternal healing after harvesting of bilateral internal thoracic arteries in not only healthy but also diabetic rats.[17,18] We also reported that prevascularization with gelatin microspheres containing this angiogenic factor can enhance the benefits of cardiomyocyte transplantation.[19] On the basis of these observations, we considered a new strategy for revascularization of severely diseased and tiny coronary arteries: (1) use of a healthy large-bored donor artery, such as the gastroepiploic artery (GEA), located near the ischemic area and (2) stimulation of angiogenesis from this donor artery soon after administration of an angiogenic factor. In other words, the strategy is a revival of the classic method, except that modern biotechnology is used (biologic coronary artery bypass grafting, or Bio-CABG). The purpose of this study was to demonstrate the feasibility of creating vascular communication between tiny coronary arteries and an extracardiac artery without surgical anastomosis by suitable placement of the artery and use of an angiogenic factor.

Material and Methods

Preparation of Gelatin Hydrogel Sheet Incorporating bFGF

Gelatin with an isoelectric point of 4.9 was isolated from bovine bone collagen by an alkaline process with calcium hydroxide (Nitta Gelatin Co, Osaka, Japan). The weight-average molecular weight of the gelatin was 99,000 d when measured by gel filtration chromatography relative to a standard polyethylene glycol sample. Human recombinant bFGF with an isoelectric point of 9.6 was obtained from Kaken Pharmaceutical Co (Tokyo, Japan). Gelatin hydrogel sheets were prepared as described previously elsewhere.[17,20] The sheets were freeze-dried and then impregnated with an aqueous solution containing 100 μg bFGF to obtain gelatin hydrogels with incorporated bFGF. The prepared hydrogel sheets were 5 × 5 mm square and 0.7 mm thick. All experimental processes were conducted under sterile conditions.

Surgical Procedure

Thirty-five Japanese white rabbits weighing 3.5 to 4.2 kg were used. All animal procedures were conducted in accordance with the "Guide for the Care and Use of Laboratory Animals" (http://www.nap.edu/catalog/5140.html). All studies were approved by the Animal Research Committee of Kyoto University School of Medicine.

After intravenous injection of sodium pentobarbital (30 mg/kg), oral intubation was performed, and the animals received mechanical ventilation (model 683; Harvard Apparatus, South Natick, Mass) at a tidal volume of 15 mL and a minute ventilation rate of 80. General anesthesia was maintained with 1.5% to 2.0% isoflurane mixed with oxygen. The heart and omentum were exposed through a median sternotomy and laparotomy. The major branch of the circumflex artery was permanently ligated with 4-0 polypropylene suture to create acute myocardial infarction (MI). Lidocaine (1 mg/kg) was administered intravenously before the completion of this procedure. Careful inspection was maintained for 10 minutes after the ligation. Ischemia was confirmed by blanching downstream of the ligation and by persistent ST elevation on the electrocardiogram. The omentum was taken out from the peritoneal space into the mediastinum, preserving the arch structure of the GEA. The animals were divided into four groups that received different types of adjunct therapy as follows: group N (n = 7, control) received no additional treatment after creation of the MI; in group G (n = 8) the omentum including the GEA was wrapped around the infarcted area; in group F (n = 10) a gelatin hydrogel sheet incorporating 100 μg bFGF was placed over the epicardium of the infarcted area; and in group FG (n = 10) a gelatin hydrogel sheet incorporating 100 μg bFGF was placed over the epicardium of the infarcted area, followed by omental wrapping (combined therapy). The bFGF-impregnated hydrogel sheets were fixed to the surface of the heart by stitching with 5-0 polypropylene suture. Before the incision was closed with discontinuous tissue layers, residual air was evacuated from the thorax through silicone tubing attached to a 10-mL syringe. All rabbits were awake within 1 hour after the operation and were kept in an air-conditioned room that was cleaned daily. The rabbits were given free access to water and food thereafter. All animal handling and experiments were conducted in a gentle manner to minimize stress and discomfort to the rabbits, in compliance with the "Guidelines for Use of Laboratory Animals at Kyoto University."

Echocardiographic Measurements

A commercially available echocardiograph (model SSH-260A Ultrasound System; Toshiba Medical, Inc, Tokyo, Japan) including a 7.5-MHz pediatric transducer was used for all studies. Echocardiographic studies were performed before the operation and at 2 and 4 weeks of follow-up. All studies were done with the animals under light anesthesia with intravenous sodium pentobarbital injection under spontaneous respiration. Global ventricular function was estimated by calculating the fractional area change (FAC) of the left ventricle (LV). Two-dimensional M-mode midventricular

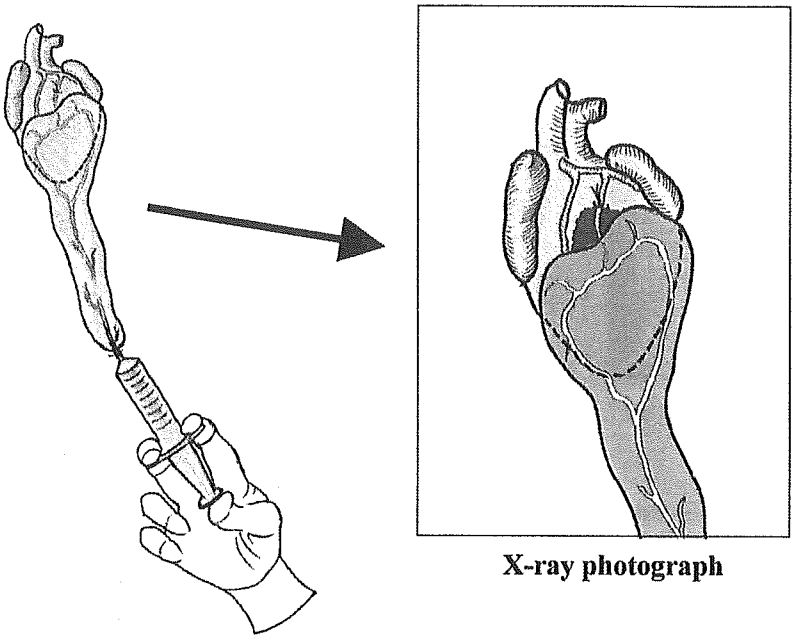

Figure 1. Schema of postmortem angiography. Contrast medium is injected into GEA through small cannula manually inserted through celiac artery. X-ray photograph is taken as in illustration *(right).*

short-axis images were obtained through a right parasternal approach to determine the FAC by tracing frame by frame throughout the entire cardiac cycle. For each measurement, three consecutive cardiac cycles were averaged. All analyses were done by another observer (K.D.), who was blinded to treatment groups.

Postmortem Angiography

Communication between the coronary arteries and branches of the GEA in the omentum was evaluated by postmortem angiography at 4 weeks after the operation in groups G and FG. After intubation, relaparotomy was performed, taking care to avoid injuring the omentum. A 24-mm venous catheter was inserted through the celiac artery, which forms the root of the GEA, and fixed. The chest was reopened to expose the heart wrapped with the omentum. The rabbits were killed with an overdose of pentobarbital, and then the heart and omentum were removed en bloc. A 20-mL portion of heparinized physiologic sodium solution was flushed through the venous catheter into the GEA.

Angiography was performed with an x-ray angiography system (DFW-10B; Toshiba Medical). Angiograms were taken four times every 3 seconds after the start of manual injection of nonionic contrast medium for later analysis (Figure 1). A 3-mL portion of contrast medium was injected by hand for 5 seconds in all cases. Quantitative angiographic analysis of collateral vessel development was performed with a grid overlay composed of 2.5-mm diameter circles arranged at random in the LV distant from the GEA itself. The total number of grid intersections in the LV area, as well as the total number of intersections crossed by a contrast-opacified artery, were counted in a single-blind manner. An angiographic score was calculated for each film as the ratio of grid intersections crossed by opacified arteries divided by the total number of grid intersections in the LV area.

Histologic Analysis of MI Area and Arteriolar Density

After the angiography, the heart was cut into 2-mm thick slices from apex to base in groups G and FG. In groups N and F, the same procedure was performed after the animals had been killed. The slices were immersed in buffered triphenyltetrazolium chloride (TTC) solution and then photographed, and infarct size was calculated with image analysis software (NIH Image 1.61; National Institutes of Health, Bethesda, Md). Each image was analyzed five times and averaged. Infarct size was defined as the percentage of the infarction area within the total area of the LV in each histologic section. As dimensional analysis of the infarction area, three equally spaced measurements of infarct wall from same slices were performed to determine average wall thickness. At the same time, endocardial circumferential length of LV and the scar were measured. For both infarct size and dimensional measurements, the observer was blinded to treatment group. The midcavity area, not used for TTC immersion, was fixed in 4% paraformaldehyde, embedded in paraffin, and cut into sections 5 μm thick. The sections were stained with Masson trichrome to evaluate collagen deposition in comparison with TTC staining.

Other midcavity sections fixed in 4% paraformaldehyde were stained with a monoclonal antibody against α–smooth muscle actin (Sigma, St Louis, Mo), followed by incubation with anti-mouse immunoglobulin G (whole molecule). Tetramethylrhodamine isothiocyanate–conjugated secondary antibody (Sigma) was used to detect α–smooth muscle cells of arterioles. The sections were counterstained with hematoxylin, eosin, or both. The numbers of arterioles were counted at the infarction border zone under fluorescence microscopy ($\times$100) to determine the arteriolar density. Five fields from one section were randomly selected for the arteriole counts. An arteriole was defined as a vessel with a diameter of 20 to 100 μm. Quantification was performed in a

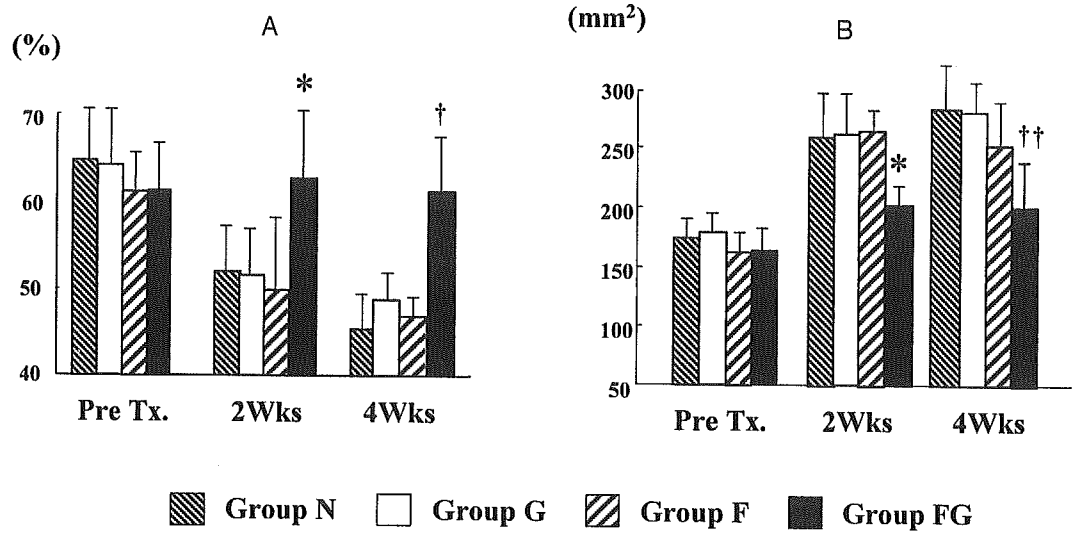

Figure 2. FAC (A) and LVEDA (B) assessed by echocardiography before operation and at 2 and 4 weeks' follow-up. *Pre Tx,* Before treatment. *Asterisk* indicates $P < .05$ versus groups N, G, and F; *dagger* indicates $P < .001$ versus groups N, G, and F; *two daggers* indicate $P < .01$ versus groups N, G, and F.

blinded manner with a minimum of three sections for each animal. All animals were used for the analysis.

Statistical Analysis

Results are expressed as mean ± SD. Comparisons of echocardiography data among the groups were performed by 2-way analysis of variance (ANOVA). Comparisons of other data among the groups were conducted by 1-way factorial ANOVA. If significance was found for a group, a time effect, or a group-by-time interaction, differences between groups at the same point in time were assessed with 1-way ANOVA followed by post hoc comparisons, when appropriate, with the Student-Newman-Keuls method. Statistical analyses were performed with Statview for Windows version 5.0 (SAS Institute Inc, Cary, NC).

Results

Global Cardiac Function Assessed by Echocardiography

Figure 2 shows the changes in FAC and LV end-diastolic area (LVEDA). None of the FAC and LVEDA values in any of the groups were different before the operation. Two-way ANOVA for FAC showed strong group and time effects and a high group-by-time interaction (respectively $F = 9.4$, $P < .0001$, $F = 20.0$, $P < .0001$, and $F = 4.1$, $P = .0014$).

At 2 weeks after the procedure, FAC values in group FG were significantly higher than in groups N, G, and F ($P = .03$, $P = .04$, and $P = .02$, respectively). At 4 weeks, group FG showed higher FAC values than did the other three groups (group FG 65 ± 7, group N 46 ± 1, $P = .0004$, group G 51 ± 7; $P = .002$, and group F 46 ± 4, $P = .0005$).

The changes in LVEDA values, which indicate the loading conditions of LV, showed a pattern similar to that of FAC. At 4 weeks, LVEDA was significantly lower in group FG than in groups N and G. No difference reached significance, but LVEDA in group FG had a tendency to be low compared with group F (group FG 198 ± 45 mm², group N 280 ± 50 mm²; $P < .001$, group G 275 ± 35 mm², $P = .003$, and group F 250 ± 52 mm², $P = .06$).

Communication Between Coronary Arteries and the GEA in Terms of Angiographic Assessment and Angiographic Score

Angiography was performed in 7 animals in each of groups FG and G. Communication from the GEA was created to the coronary artery though rich collaterals in all 7 animals of group FG. On the other hand, the circumflex artery was identified through poor collaterals in 2 of 7 animals of group G. Representative angiograms recorded from groups FG and G are shown in Figure 3, *A*. The angiographic score in group FG (0.82 ± 0.13) was significantly ($P < .001$) higher than that in group G (0.1 ± 0.11; Figure 3, *B*).

Infarct Size and Dimensional Analysis of MI

MI was recognized at the anterolateral wall of the LV, posterolateral wall of the LV, or both in all groups, although there was difference in the infarct size. The infarct ratios determined by analysis of TTC staining in groups N, G, and F were 23% ± 2%, 19 ± 7%, and 16% ± 5%, respectively, which were significantly higher than that in group FG (10% ± 3%) ($P < .001$, $P = .001$, and $P = .04$ for each of the groups; Figure 4). There was no difference between groups G and F. MI size was reduced to a greater extent in group F than in group N ($P = .03$). Although there was no significant difference in average wall thickness in all

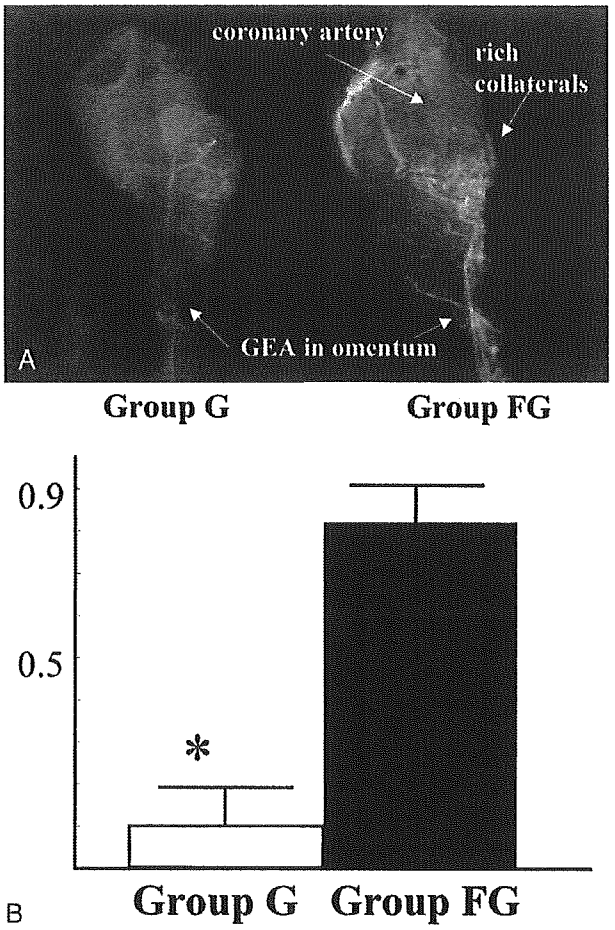

Figure 3. A, Representative postmortem angiogram in groups with omental wrapping (group G) and omental wrapping with bFGF (group FG). *Left,* in group G, GEA in omentum is opacified, but no communication to coronary arteries is identified. *Right,* in group FG, numerous collaterals are created between GEA and occluded coronary arteries. B, Angiographic score calculated by postmortem angiographic analysis in groups with omental wrapping (group G) and omental wrapping with bFGF (group FG). *Asterisk* indicates $P < .001$ versus group FG.

groups, circumferential lengths of LV and the scar were lower in group FG than the other three groups (Table 1).

Immunohistochemical Analysis of New Vessel Formation

Immunohistochemical staining for anti–α–smooth muscle actin revealed that the number of arterioles was increased in the following order: group FG (23 ± 5) more than group F (14 ± 3) more than group G (10 ± 1) more than group N (4 ± 2), with each of the differences being significant (Figure 5, *A*). Figure 5, *B,* shows representative photomicrographs (original magnification ×100) for groups G and FG.

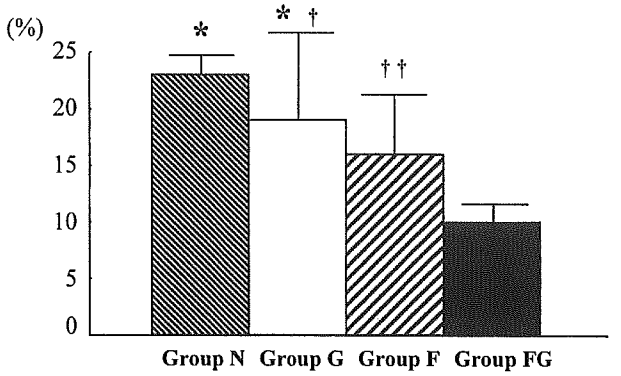

Figure 4. Infarction ratios (% of whole LV) determined by analysis of TTC staining. *Asterisk* indicates $P < .01$ versus group FG; *dagger* indicates $P < .05$ versus group F; *two daggers* indicate $P < .05$ versus group FG.

TABLE 1. Dimensional analysis of the scar

	LV circumferential length (mm)	Circumferential length of scar (mm)	Infarct wall thickness (mm)
Group N	61 ± 8	27 ± 4	1.9 ± 0.4
Group G	58 ± 5	28 ± 5	2.1 ± 0.7
Group F	56 ± 8*	24 ± 4	2.0 ± 0.2
Group FG	48 ± 3†	16 ± 2‡	2.5 ± 0.4

*$P < .005$ versus group FG.
†$P < .001$ versus groups N and F.
‡$P < .001$ versus groups N, G, and F.

Discussion

Multiple experimental and clinical studies have obtained promising results with therapeutic angiogenesis as an alternative to conventional percutaneous coronary intervention or CABG for coronary artery disease that otherwise would have no treatment options.[2-9] If, however, the donor coronary artery was too far from the target area, too tiny, or diseased or stenosed, conventional therapeutic angiogenesis might not be sufficiently efficacious. Therefore we have proposed a revival of the classic revascularization technique of omentopexy by adding a modern biotechnologic tool, slow release of an angiogenic factor, as an optional strategy for therapeutic angiogenesis.

In this study, the combined therapy involving omentopexy and bFGF administration (group FG) preserved cardiac function better than was seen in the other groups, not only by reducing MI size but also by increasing the number of arterioles. Although myocardial blood flow and hemodynamics were not measured, objective data including postmortem angiography suggested that numerous functional neovessels were connected to the coronary artery from the donor artery. However, the true mechanism of this efficacy was not clear. The pathogenesis of MI, which can be acutely completed within 24 hours, could not be altered by angio-

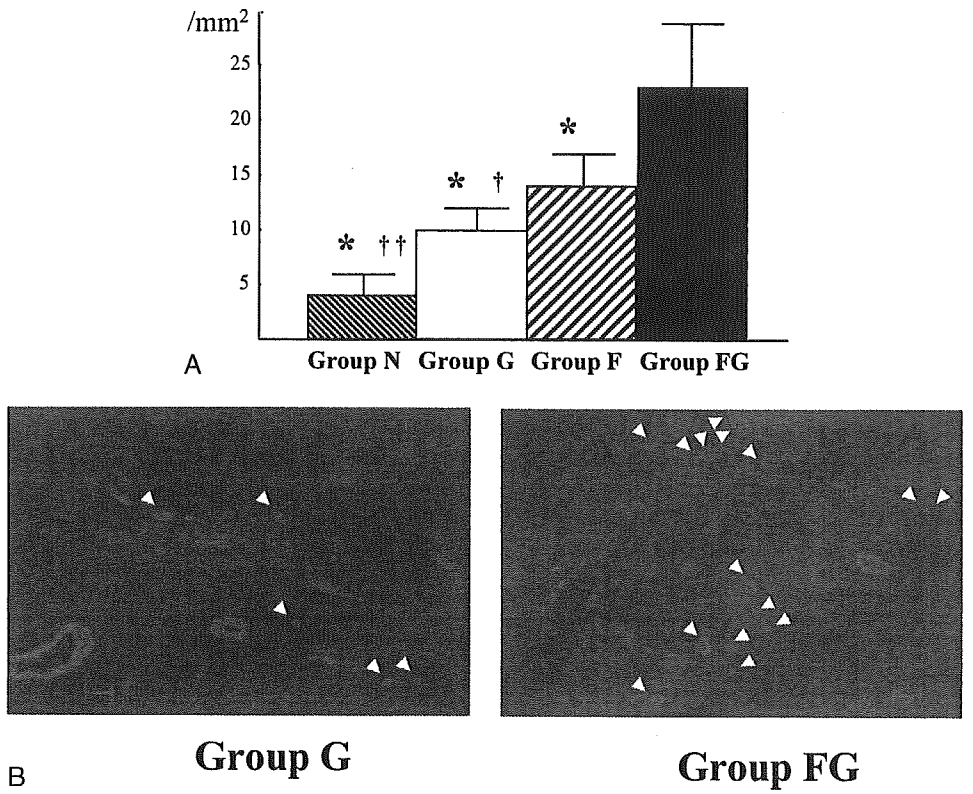

Figure 5. A, Number of arterioles counted by immunohistochemical staining. Arteriole was defined as vessel with diameter of 20 to 100 μm. *Asterisk* indicates $P < .001$ versus group FG; *two daggers* indicate $P < .01$ versus group G; *dagger* indicates $P < .05$ versus group F. B, Representative immunohistochemical staining photos (original magnification ×100) in groups with omental wrapping (group G) and omental wrapping with bFGF (group FG). Arterioles in border zone of MI are stained by anti–α–smooth muscle actin. *White arrows* indicate arterioles. *Blue bar* at lower right is scale of 100 μm.

genesis. It is possible that the Bio-CABG altered the remodeling process of scar tissue clearance in this study. Preservation of better cardiac function and reduction in MI size may be related to differences in the size of the ventricle caused by altering the remodeling process. The results of dimensional analysis of scar and difference of loading condition were consistent with this presumption.

Omentum including the GEA has classically been used for surgical treatment of not only ischemic heart disease but also complex cardiothoracic problems[21,22] because the omentum possesses a rich blood and lymph supply and has the additional benefit of producing an angiogenic factor, vascular endothelial growth factor.[23] In addition to this unique functional character, an omental flap has the advantage of being able to reach and wrap a target organ entirely because of its intrinsic structure. The GEA has become firmly established as an in situ graft conduit with low morbidity, including abdominal complications.[24] The weak point of omentopexy for myocardial revascularization is its slow and insufficient angiogenesis, similar to that of the Vineberg operation. In this study, we added a bFGF-containing gelatin sheet to the omental wrapping, and this was found to accelerate angiogenesis effectively relative to omentopexy alone.

Previous studies have shown that gene encoding, virus mediation, and direct injection into the coronary artery or intrapericardially are useful mechanisms for delivering an angiogenic factor to its target.[2-7] The method used for delivering angiogenic protein in this study was technically simpler and more reliable, and, because it did not involve genes or viruses, it would also be less likely to have adverse effects on a patient. We have reported that prevascularization with bFGF-containing microspheres enhanced the benefits of cardiomyocyte transplantation without increasing the serum level of bFGF (no systemic effects).[19] Although the technique of delivering bFGF in this study, gelatin sheets attached to the epicardium, differed from injection of beads into the myocardium, the sheets were made of the same material as the beads, and the rate of bFGF release was almost the same. We therefore consider this delivery

method with gelatin hydrogel to be potentially excellent and widely applicable to other growth factors.

In a clinical setting, Bio-CABG will probably be applicable for treatment of diffuse coronary artery disease that cannot be treated by percutaneous coronary intervention or conventional CABG. This type of coronary artery disease is often recognized in patients receiving hemodialysis or those with severe diabetes mellitus. Even in the era of drug-eluting stents, tiny coronary arteries remain a difficult target for interventional catheters. Therefore Bio-CABG has the potential to be a promising new avenue for so-called no option patients with severe coronary disease.

This study was limited as a means of assessing therapeutic angiogenesis in the sense that the acute MI model differs from the clinical situation. Furthermore, myocardial blood flow and hemodynamic effects were not assessed. Angiography and histologic examination do not establish evidence of increased perfusion. Therefore in a future study we are planning to try to estimate myocardial blood flow and the practical efficacy of Bio-CABG directly with the chronic ischemia model in a large animal. Another limitation is that the method for delivering bFGF in this study may not be as good as our previous technique of implanting biodegradable capsules or other techniques,[8,9] because the attachment of the gelatin sheet to the epicardium may not provide sufficient angiogenic stimuli to the mid or endocardial region of the LV. The omental wrapping may not provide long-term perfusion of the myocardium, and short-term benefits would be anticipated with this procedure. A small MI area was produced in this study even in the control animals. This finding may be related to the use of TTC staining for a short time, which may reduce the accuracy of infarct identification.

In conclusion, we have demonstrated that Bio-CABG can be used to create marked communication between tiny coronary arteries and an extracardiac artery by administration of slow-release bFGF, without surgical anastomosis. This new concept, in which modern biotechnology has been used to revive a classic operation, has the potential to offer revascularization for patients with coronary artery disease who have no other treatment options.

References

1. Lytle BW, Blackstone EH, Loop FD, Houghtaling PL, Arnold JH, Akhrass R, et al. Two internal thoracic artery grafts are better than one. *J Thorac Cardiovasc Surg.* 1999;117:855-72.
2. Rajanayagam MA, Shou M, Thirumurti V, Lazarous DF, Quyyumi AA, Goncalves L, et al. Intracoronary basic fibroblast growth factor enhances myocardial collateral perfusion in dogs. *J Am Coll Cardiol.* 2000;35:519-26.
3. Shou M, Thirumurti V, Rajanayagam S, Lazarous DF, Hodge E, Stiber JA, et al. Effect of basic fibroblast growth factor on myocardial angiogenesis in dogs with mature collateral vessels. *J Am Coll Cardiol.* 1997;29:1102-6.
4. Lopez JJ, Laham RJ, Stamler A, Pearlman JD, Bunting S, Kaplan A, et al. VEGF administration in chronic myocardial ischemia in pigs. *Cardiovasc Res.* 1998;40:272-81.
5. Banai S, Jaklitsch MT, Shou M, Lazarous DF, Scheinowitz M, Biro S, et al. Angiogenic-induced enhancement of collateral blood flow to ischemic myocardium by vascular endothelial growth factor in dogs. *Circulation.* 1994;89:2183-9.
6. Tio RA, Tkebuchava T, Scheuermann TH, Lebherz C, Magner M, Kearny M, et al. Intramyocardial gene therapy with naked DNA encoding vascular endothelial growth factor improves collateral flow to ischemic myocardium. *Hum Gene Ther.* 1999;10:2953-60.
7. Mack CA, Patel SR, Schwarz EA, Zanzonico P, Hahn RT, Ilercil A, et al. Biologic bypass with the use of adenovirus-mediated gene transfer of the complementary deoxyribonucleic acid for vascular endothelial growth factor 121 improves myocardial perfusion and function in the ischemic porcine heart. *J Thorac Cardiovasc Surg.* 1998;115:168-76.
8. Laham RJ, Sellke FW, Edelman ER, Pearlman JD, Ware JA, Brown DL, et al. Local perivascular delivery of basic fibroblast growth factor in patients undergoing coronary bypass surgery: results of a phase I randomized, double-blind, placebo-controlled trial. *Circulation.* 1999; 100:1865-71.
9. Ruel M, Laham RJ, Parker JA, Post MJ, Ware JA, Simons M, et al. Long-term effects of surgical angiogenic therapy with fibroblast growth factor 2 protein. *J Thorac Cardiovasc Surg.* 2002;124:28-34.
10. O'Shaughnessy L. Surgical treatment of cardiac ischemia. *Lancet.* 1937;232:185-94.
11. Vineberg AM, Miller G. Internal mammary coronary anastomoses in surgical treatment of coronary artery insufficiency. *Can Med Assoc J.* 1951;64:204-10.
12. Vineberg AM. Revascularization of the entire heart by internal mammary artery implantation, epicardiectomy and free omental graft. *Can Med Assoc J.* 1966;94:378-85.
13. Vineberg AM, Kato Y, Pirozynski WJ. Experimental revascularization of the entire heart. Evaluation of epicardiectomy, omental graft, and/or implantation of the internal mammary artery in preventing myocardial necrosis and death of the animal. *Am Heart J.* 1966;72:79-93.
14. Friedbacker K. Omentum as source of nutrition to experimentally produced myocardial ischemia. *Surg Gynecol Obstet.* 1942;75:110-3.
15. Vineberg A. Revascularization of the right and left coronary arterial systems. Internal mammary artery implantation, epicardiectomy and free omental graft operation. *Am J Cardiol.* 1967;19:344-53.
16. Streider JW, Clute HM, Graubiel A. Cardioomentopexy in the treatment of angina pectoris. *N Engl J Med.* 1940;222:41-3.
17. Iwakura A, Tabata Y, Miyao M, Ozeki M, Tamura N, Ikai A, et al. Novel method to enhance sternal healing after harvesting bilateral internal thoracic arteries with use of basic fibroblast growth factor. *Circulation.* 2000;102(19 Suppl 3):III307-11.
18. Iwakura A, Tabata Y, Tamura N, Doi K, Nishimura K, Nakamura T, et al. Gelatin sheet incorporating basic fibroblast growth factor enhances healing of devascularized sternum in diabetic rats. *Circulation.* 2001;104(12 Suppl 1):I325-9.
19. Sakakibara Y, Nishimura K, Tambara K, Yamamoto M, Lu F, Tabata Y, et al. Prevascularization with gelatin microspheres containing basic fibroblast growth factor enhances the benefits of cardiomyocyte transplantation. *J Thorac Cardiovasc Surg.* 2002;124:50-6.
20. Tabata Y, Nagano A, Ikada Y. Biodegradation of hydrogel carrier incorporating fibroblast growth factor. *Tissue Eng.* 1999;5:127-38.
21. Shrager JB, Wain JC, Wright CD, Donahue DM, Vlahakes GJ, Moncure AC, et al. Omentum is highly effective in the management of complex cardiothoracic surgical problems. *J Thorac Cardiovasc Surg.* 2003;125:526-32.
22. Levashev YN, Akopov AL, Mosin IV. The possibilities of greater omentum usage in thoracic surgery. *Eur J Cardiothorac Surg.* 1999; 15:465-8.
23. Zhang QX, Magovern CJ, Mack CA, Budenbender KT, Ko W, Rosengart TK. Vascular endothelial growth factor is the major angiogenic factor in omentum: mechanism of the omentum-mediated angiogenesis. *J Surg Res.* 1997;67:147-54.
24. Suma H, Amano A, Horii T, Kigawa I, Fukuda S, Wanibuchi Y.

Gastroepiploic artery graft in 400 patients. *Eur J Cardiothorac Surg.*. 1996;10:6-10.

Discussion

Dr Hiroyuki Tsukui *(Pittsburgh, Pa).* I have two questions. First, how long does the bFGF effect last? Second, what is an appropriate volume? Do you use 100 μg?

Dr Ueyama. We use the administration method of bFGF by gelatin hydrogel sheet. We used that dose of, as you say, 100 μg bFGF only in this study. But in another study we have already reported that a 100-μg dose of bFGF was enough to inducing angiogenesis for another target organ.

Dr Tsukui. So do you mean that a flow rate of 100 μg is appropriate? Or if you used it 12 or more weeks at 200 μg or another dose, would that be better for revascularization?

Dr Ueyama. I don't have an exact answer to your question now, but I'd guess that one would not need to use more than 100 for FGF for better effect.

Dr Andrew S. Wechsler *(Philadelphia, Pa).* Did you happen to look and see how deep in the myocardium the new blood vessels went? Did they reach the subendocardial surface or the mid myocardium, or was it primarily an epicardial blush?

Dr Ueyama. I think the results of angiography suggested that the new vessel from the GEA passed through the epicardium and myocardium and bypassed to the coronary artery.

Dr Virna Sales *(Boston, Mass).* Would you be able to see a prospective microencapsulating this bFGF with a hydrogel and have that kind of delivery?

Dr Ueyama. Yes, we did. The material is the same that we used in this study.

Dr Sales. But would that be possible to microencapsulate this?

Dr Ueyama. In another study we used microspheres including bFGF injected into myocardium. Many angiogenesis occurred in the myocardium between each coronary artery but not from an extracardiac donor artery.

Dr Sales. What is the degradation time of this hydrogel? You said it was biodegradable.

Dr Ueyama. It takes about 7 to 10 days for complete degradation.

GENES, CHROMOSOMES & CANCER 40:120–132 (2004)

Gene Expression Profiling and Identification of Novel Prognostic Marker Genes in Neuroblastoma

Junko Takita,[1] Masami Ishii,[1,2] Shuichi Tsutsumi,[1,2] Yukichi Tanaka,[3] Keisuke Kato,[3] Yasunori Toyoda,[4] Ryoji Hanada,[5] Keiko Yamamoto,[5] Yasuhide Hayashi,[1,6*] and Hiroyuki Aburatani[2*]

[1]Department of Pediatrics, Graduate School of Medicine, University of Tokyo, Tokyo, Japan
[2]Genome Science Division, Research Center for Advanced Science and Technology, University of Tokyo, Tokyo, Japan
[3]Division of Pathology, Kanagawa Children's Medical Center, Kanagawa, Japan
[4]Division of Hematology, Kanagawa Children's Medical Center, Kanagawa, Japan
[5]Division of Hematology/Oncology, Saitama Children's Medical Center, Saitama, Japan
[6]Gunma Children's Medical Center, Gunma, Japan

To investigate the various genetic characteristics of and differences between early- and advanced-stage neuroblastoma (NB) and to identify candidate genes involved in NB progression, we performed DNA microarray analysis on 20 primary tumors. Two-way clustering analysis based on the expression pattern of approximately 500 of 1,700 genes revealed genetic subgroups in these NB tumors. Although 9 of the 13 early-stage tumors (69%) and 4 of the 6 advanced-stage tumors (67%) were classified as being in the same cluster, the remaining tumors showed different expression profiles. This indicates that both the early- and advanced-stage tumors were heterogeneous. Based on the microarray data, we identified the *BIRC*, *CDKN2D*, and *SMARCD3* genes as those that are predominantly expressed in either the early or the advanced stage of NB. These genes have been reported to be associated with apoptosis, cell cycles, and the transcriptional activator, respectively. To better assess the prognostic value of the expression of these genes in NB, real-time polymerase chain reaction was carried out on 50 primary tumors. The expression of both the *BIRC3* and *CDKN2D* genes was significantly higher in the early-stage group than in the advanced-stage group ($P = 0.002$ and 0.003, respectively), whereas the expression of the *SMARCD3* gene was significantly reduced in the early-stage group ($P = 0.02$). Therefore, the *BIRC*, *CDKN2D*, and *SMARCD3* genes are possible candidates for being novel prognostic markers for NB.

INTRODUCTION

Chromosomal abnormalities including the gain and loss of chromosomal segments frequently occur in tumor cells (Knudson, 2001). These changes may result in alterations in the expression level of numerous genes. It is therefore of considerable interest to assess genomewide gene expression patterns to determine candidate oncogenes and tumor-suppressor genes for human cancers.

Neuroblastoma (NB) is a common childhood malignant solid tumor arising from primitive neural-crest cells, and causes 15% of cancer-related deaths in children (Brodeur et al., 1997). Patients with early-stage NB, particularly those detected by a mass screening program, are known to have a good prognosis, and the tumors of these patients possess the ability to differentiate and/or regress spontaneously (Yamamoto et al., 1998). In contrast, patients with advanced-stage NB still have a poor prognosis despite recent developments in treatment (Brodeur et al., 1997). This suggests the presence of genetic mechanisms that are quite different between early- and advanced-stage NB.

MYCN oncogene amplification and high levels of both *TRKA* and *RASH* expression have been known to be reliable prognostic markers for NB (Brodeur et al., 1984; Nakagawara et al., 1993; Tanaka et al., 1998). Recently, it also was reported that high-level expression of *RASH* in NB cells is associated with nonapoptotic programmed cell death (Kitanaka et al., 2002). However, because *MYCN* amplification occurs in approximately half the cases of advanced NB, it has been suggested that *MYCN*-independent pathways exist in NB pro-

Supported by: Ministry of Health and Welfare of Japan grant-in-aid for Cancer Research; Ministry of Education, Culture, Sports, Science and Technology, Japan, grants-in-aid for Scientific Research on Priority Areas and for Scientific Research (B) and (C).

*Correspondence to: Yasuhide Hayashi, M.D., Vice Director, Gunma Children's Medical Center, 779 Shimohakoda, Kitatachibana, Gunma 377-8577, Japan. E-mail: hayashiy-tky@umin.ac.jp or Hiroyuki Aburatani, M.D., Genome Science Division, Research Center for Advanced Science and Technology, University of Tokyo, 4-6-1 Komaba, Meguro-ku, Tokyo 153-8904, Japan.
E-mail: haburata-tky@umin.ac.jp

J. Takita and M. Ishii contributed equally to this article.

Received 29 July 2003; Accepted 28 January 2004
DOI 10.1002/gcc.20021
Published online 26 March 2004 in
Wiley InterScience (www.interscience.wiley.com).

gression (Brodeur et al., 1997; Schwab, 1997). *TRKA* and *RASH* expression are inversely correlated with *MYCN* amplification, indicating that these genes are not prognostic factors independent of *MYCN* amplification (Nakagawara et al., 1993; Tanaka et al., 1998). Previously, we reported that chromosome arms 2q, 9p, and 18q, in addition to 1p, 11q, and 14q, were frequently deleted in NB (Takita et al., 1995, 1997, 2000). Furthermore, we reported that the *caspase 8* gene, on chromosome band 2q33, the *CDKN2A* (*p16*) gene, on chromosome band 9p21, and the *DCC* gene, on chromosome band 18q21, might be candidate tumor-suppressor genes that are inactivated in NB (Takita et al., 1995, 1997, 1998, 2001; Kong et al., 1997; Teitz et al., 2000). However, alterations of these genes had been detected in only a limited fraction of NBs (Kong et al., 1997; Takita et al., 1997, 1998, 2001). More recently, using polymerase chain reaction (PCR), we and other groups found a ~480-kb homozygous deletion on chromosome segment 1p36.2 in an NB cell line, which, according to high-density STS-content map spanning, is approximately 35 Mb on 1p35–36 (Ohira et al., 2000; Chen et al., 2001), and *KIF1B-α*, *KIF1B-β*, and *DFF45* genes were identified within the deleted region (Yang et al., 2001a, 2001b; Chen et al., 2003). Although we analyzed these genes in NB, we found no evidence that either gene was a candidate tumor-suppressor gene of NB (Yang et al., 2001a, 2001b). Thus, the genetic differences between favorable and unfavorable NB and the molecular genetic events involved in the genesis and progression of NB are not fully understood.

Recently, doing large-scale expression profiling has become possible with the development of array technologies (Ishii et al., 2000; Gershon, 2002). Gene expression on a large scale now can be measured at one time, and comparisons among different tumor characteristics are expected to provide better insights into the development and/or progression of tumors (Ishii et al., 2000; Gershon, 2002). To investigate further the patterns of differential gene expression in early- and advanced-stage NB and to identify the target genes for NB progression, we carried out DNA microarray analysis on primary NB tumors by using an Affymetrix Human Cancer G110 array (Santa Clara, CA) representing approximately 1,700 cancer-associated genes. To assess further the expression of several genes showing differential expression patterns in early- and advanced-stage NB, we also performed quantitative real-time PCR analysis on 50 primary NB tumors.

MATERIALS AND METHODS

Tumor Samples

Fifty tumor specimens were randomly obtained at surgery or biopsy from NB patients who had been admitted to the Kanagawa Children's Medical Center and the Saitama Children's Medical Center between November 1992 and May 1999. Informed consent was obtained from both parents of each patient. Of the 50 tumors, 20 were used in microarray analysis, mainly because of the high quality of the RNA obtained from the tumor samples. The clinicopathologic findings of these 20 cases are listed in Table 1. The patients were staged according to the classification of the International Neuroblastoma Staging System (Smith et al., 1989). Of the 50 cases, 14 were classified as stage 1, 6 as stage 2, 13 as stage 3, 14 as stage 4, and 3 as stage 4S. Twenty-eight patients (56%) were infants under 1 year old at diagnosis, and 22 patients (44%) were more than 1 year old. Twenty-three (46%) of the 50 cases were found in a mass screening program (Yamamoto et al., 1998). *MYCN* amplification was detected in 4 (8%) of the 50 cases. All patients were followed up for at least 19 months and for up to 52 months, with a median duration of follow-up of 38 months. Five (10%) of the 50 patients died, and of the 20 cases examined by DNA array analysis, 3 (15%) died. Patients with NB at stage 1, 2, or 4S were treated with either surgery alone or surgery plus chemotherapy that mainly consisted of vincristine and cyclophosphamide without radiotherapy. Patients with stage-3 or -4 NB were treated with multidrug chemotherapy consisting of cyclophosphamide, doxorubicin, cisplatinum, and etoposide with or without surgery, radiotherapy, and hematopoietic stem-cell transplantation (Kaneko et al., 1999).

Tumor Cell Lines

We used 27 NB cell lines: NB-1, NB-9, NB-16, NB-19, NB-69, LAN-1, LAN-2, LAN-5, SCMC-N2, SCMC-N3, SCMC-N4, SCMC-N5, SJNB-1, SJNB-2, SJNB-4, SJNB-5, SJNB-7, SJNB-8, TGW, IMR-32, GOTO, CHP-134, NH-12, NBL, SK-N-SH, NBTU1, and SCCH-26. Four of them (SCMC-N2, SCMC-N3, SCMC-N4, and SCMC-N5) were established in our laboratory (Kong et al., 1997; Yang et al., 2000). Six SJNB cell lines (SJNB-1, SJNB-2, SJNB-4, SJNB-5, SJNB-7, SJNB-8) and NBTU1 (Inoue et al., 1997) were generous gifts from Dr. A. T. Look and Dr. A. Inoue, respectively. The other cell lines were obtained from the Japanese Cancer Resource Cell

TABLE I. Clinical Data of Cases with Neuroblastoma Used in the Microarray Analysis

Case No.	Age	Stage	Diagnosis	Histology	*MYCN* Amplification	Survival
1	7m	1	MS	NBL poorly dif.	−	3y +
2	6m	1	MS	NBL dif.	−	5y +
3	2y3m	1	C	GN	−	1y2m +
4	1y	1	C	NBL poorly dif.	−	1y10m +
5	11m	1	MS	NBL poorly dif.	−	3y8m +
6	1y	1	MS	NBL dif.	−	4y5m +
7	1y6m	1	C	GNB intermixed.	−	2y +
8	10m	1	C	GNB intermixed.	−	2y +
9	7m	1	MS	NBL dif.	−	9y8m +
10	3m	2	C	GNB intermixed.	−	4y3m +
11	6m	2	MS	NBL dif.	−	3y2m +
12	1y	2	MS	NBL poorly dif.	−	6y4m +
13	2y	2	C	GNB intermixed.	−	4y5m +
14	7m	4	MS	NBL poorly dif.	−	1y
15	4y	4	C	NBL dif.	+	1y2m +
16	2y	4	C	NBL poorly dif.	+	1y6m
17	1y	4	C	NBL poorly dif.	+	10m
18	7y	4	C	NBL poorly dif.	−	2y8m +
19	8y	4	C	NBL poorly dif.	−	1y10m +
20	0m	4s	C	NBL poorly dif.	−	4y3m +

MS, mass screening; C, clinical; NBL poorly dif., neuroblastoma of poorly differentiated type; NBL dif., differentiating-type neuroblastoma; GNB intermixed, ganglioneuroblastoma of intermixed type; GN, ganglioneuroma.

Bank (http://cellbank.nihs.go.jp/). All cells were maintained in RPMI 1640 (GIBCO RLB, Tokyo, Japan) medium supplemented with 10% fetal bovine serum in a humidified atmosphere containing 5% CO_2 at 37°C.

Total RNA Preparation and DNA Microarray Analysis

Total RNA was extracted from frozen tumors using Isogen reagent (Nippon Gene, Osaka, Japan) according to the manufacturer's instructions. Approximately 10 μg of total RNA from each sample was used for synthesis of biotin-labeled cRNA and hybridized to the microarray (GeneChip Human Cancer G110 array; Affymetrix, Santa Clara, CA) as described previously (Mukasa et al., 2002; Wai et al., 2002). The Human Cancer G110 array represents approximately 1,700 cancer-related genes. After washing, the arrays were stained with streptavidin-phycoerythrin (Molecular Probes, Inc., Eugene, OR), and primary data were collected by scanning with a Hewlett-Packard scanner. We used GeneChip version 3.3 software (Affymetrix, Santa Clara, CA) to calculate the average difference for each gene probe on the array, which was shown as an intensity value of the gene expression, defined by using the Affymetrix algorithm. The average difference has been shown to be a quantitative reflection of the abundance of a particular mRNA molecule in a population (Mukasa et al., 2002). To allow comparison among multiple arrays, the average differences were normalized for each array by assigning the average of the overall average difference values to 100.

Semiquantitative RT-PCR

cDNA was synthesized with oligo(dT) primer in a 20-μl reaction volume from 5 μg of total RNA by use of the SuperScript Preamplification System for first-strand cDNA synthesis (Life Technologies, Inc., Rockville, MD). Semiquantitative RT-PCR analysis of the 6 genes—*TPM4* (also called *TRKA*), *CDKN2D* (also called *p19INK4D*), *BIRC3* (also called *API2*), *DP1*, *SMARCD3* (also called *BAF60c*), *NME1* (also called *NM23-H1*), and *MYCN*—was performed on the 20 samples used for the microarray analysis. These genes were selected because of their typical expression pattern in early- and advanced-stage tumors. PCR was then performed with 0.5 μl of cDNA for 1 cycle of 95°C for 2 min, followed by 20–30 cycles of 95°C for 20 sec, 55°C for 30 sec, and 72°C for 3 min (Mukasa et al., 2002). The concentration of the cDNA was equalized by using the expression of the glyceraldehyde-3 phosphate dehydrogenase (*GAPDH*) gene as a control. PCR products were separated by electrophoresis on 1.5% agarose gels and were visualized with ethidium bromide staining. The number of PCR

TABLE 2. Primer Sequences Used in Real-Time PCR Analysis of Neuroblastoma

Genes	Sense primer sequence (5′–3′)	Antisense primer sequence (5′–3′)	Annealing temperature (°C)
BIRC2	CTGTGAACTCTACAGAATCTCT	AGTAAGAACCACTGAACAAGC	60
BIRC3	TGATCCATGGGTAGACATGC	TATTAAAGCCCATTTCCAAGGCA	58
CDKN2D	ATGCTGCTGGAGGAGGTTCG	CGGTGCTGCCAAACATCATGAC	58
SMARCD1	GTGATCATCCAAGCACTGTG	TGTGGGAGAGGCCCTATGTAT	60
SMARCD2	GTCATTGAGCTGGACAAGGAG	GTAACGGTTGCAGTTGATGTA	58
SMARCD3	ACACTTTTAACCCTGCGAAG	TCTTCACATACTGCCACAGG	60

cycles was optimized to ensure that the product intensity was within the linear phase of amplification. For each primer set, the amplification was sequenced after subcloning into the pGEM-T easy vector (Promega, Madison, WI) to confirm that the correct target gene was amplified (Mukasa et al., 2002). The signal intensity of the 6-gene expression by RT-PCR was calculated with a scanning densitometer and data analysis system (Discovery Series; Quantity One, PDI, New York, NY).

Quantitative Real-Time RT-PCR

Quantitative real-time RT-PCR analysis was performed on 50 samples with the iCycler Iq™ real-time PCR detection system (Bio-Rad Laboratories, Hercules, CA) using the SYBR® Green I dye method for doing real-time PCR (Perkin Elmer/Applied Biosystems Division, Foster City, CA). To compare the relative levels of gene expression in the NB samples, we used cDNA from a normal adult adrenal grand (Clontech, Tokyo, Japan). The real-time PCR reactions were performed in 50-μl volumes that included 5 μl of SYBR green buffer, 1 μl of cDNA template, and 2.5 μl of each primer (Nakao et al., 2000). The primers used in the real-time PCR analysis are listed in Table 2. The optional thermal-cycling condition was as follows: 40 cycles of a two-step PCR (95°C for 15 sec, 58°C or 60°C for 60 sec) after the initial denaturation (95°C for 10 min). To quantify the expression level of each gene in the tumors and in the normal samples, we generated standard curves using the known copy numbers (10 to 1×10^6) of each gene and β-*actin* transcripts, and the gene expression levels in each cDNA sample were normalized to the internal β-actin levels. The experiments were carried out twice for each data point.

Statistical Analyses

To select the genes that were differentially expressed in the early- and advanced-stage groups, we adopted the prediction value system described previously (Yeoh et al., 2002). The signal-to-noise value (S/N value) was calculated by the equation S/N value = $[\mu 1(g) - \mu 2(g)]/[\sigma 1(g) + \sigma 2(g)]$, where $[\mu 1(g), \sigma 1(g)]$ and $[\mu 2(g), \sigma 2(g)]$ denote the means and standard deviations of the log of the expression levels of gene g for the samples in groups 1 and 2, respectively. Large S/N values indicate a strong correlation between gene expression and group membership. Genes were sorted by S/N value in order to select the genes exhibiting differential expression. Principal-components analysis (PCA) was done as previously described in order to survey the overview of the distribution of the samples (Yeoh et al., 2002). The significance of the differences in the biological and clinical features of the disease within a patient group was examined using Welch's test.

RESULTS

Two-way Clustering Analysis in NB

Thirteen early-stage, 6 advanced-stage, and 1 stage-4S patient with NB were analyzed by microarray and expression data for approximately 1,700 genes. With the expression data for 496 expressed genes that passed prefiltering, two-way clustering analysis ordered according to Pearson's correlation coefficients was performed. This analysis separated the 20 samples into subsets (Fig. 1). Nine of the 13 early-stage tumors (69%) were classified into a similar expression profiling group (group 1), and 4 of 6 advanced-stage tumors (67%) were classified into another expression profiling group (group 2) in this clustering analysis. The one stage-4S tumor showed an expression pattern similar to that of group 2 tumors (Fig. 1). Classified as group 1 were 8 of 11 patients (73%) over 1 year of age and 7 of 11 patients (64%) detected by a mass screening program. In group 2 were the 3 patients who died from the sample of 20 patients, as well as 3 of 4 patients (75%) with *MYCN* amplification;

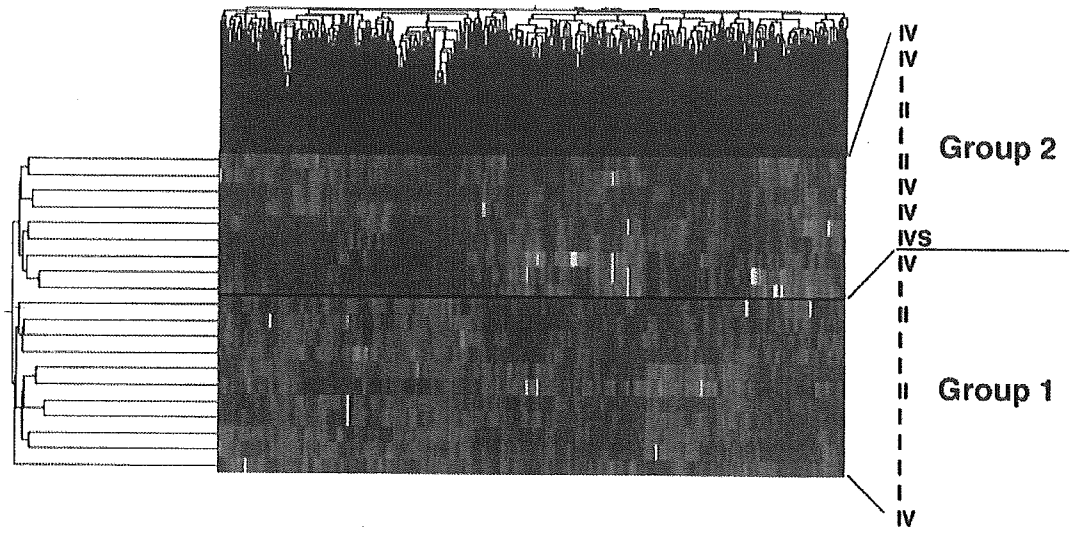

Figure 1. Two-way clustering analysis of neuroblastoma. Each column represents a gene and each row a sample. The stages of the patient samples are listed on the right. Red indicates increased gene expression and blue decreased gene expression. The expression of each gene is normalized to its median, and the dendrogram shows the degree of similarity between their expression profiles.

supplementary data are available: http://www2.genome.rcast.u-tokyo.ac.jp/NBL/supp.html.

Identification of Differentially Expressed Genes in the Early- and Advanced-Stage NB

To select the genes expressed differentially between the early- and advanced stages of NB, we used the S/N value in signal-to-noise analysis, which was recently described as useful for extracting genes expressed as uniformly high in one group and low in another (Mukasa et al., 2002). Of the 496 genes selected by S/N value, the top 30 genes showing a higher expression in the early-stage tumors are listed in Table 3, and the bottom 30 genes showing a higher expression in the advanced-stage tumors are listed in Table 4. Genes highly expressed in the early-stage group include apoptosis- or cell cycle–related genes, such as the *BIRC3* and *CDKN2D* genes (Fig. 2; Guan et al., 1996; LaCasse et al., 1998). The *TRKA* gene, known to be a prognostic marker of favorable NB (Brodeur et al., 1984; Nakagawara et al., 1993), was also detected as one of the highly expressed genes in the early-stage tumors in this study. Furthermore, we identified the *SMARCD3* gene, known to be associated with the transcriptional activator (Wang et al., 1996), as one of the genes expressed more highly in the advanced stage of NB. The *NME1* gene, whose expression has been found to in-

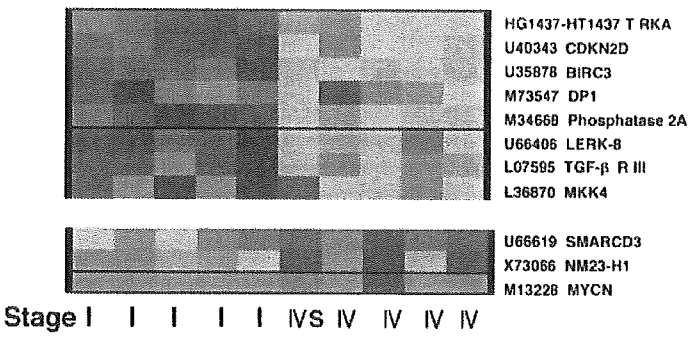

Figure 2. Genes differentially expressed in early and advanced stages of neuroblastoma. The expression level was normalized per gene. The value relative to the median among 20 samples is indicated by color: red, relatively high expression; blue, relatively low expression. The cutoff value was set at 80 for average intensity and at 2.0 for ratio. To the left of a gene's name are its Genebank association numbers.

TABLE 3. Genes Showing Higher Expression in Early-Stage Tumors

No.	Accession number	Symbol	Description	S/N value
1	L08488	*INPP1*	Inositol polyphosphate 1-phosphatase	1.936
2	M73547	*DP1*	Human polyposis locus	1.733
3	L78833	*VAT1*	Rho7 and vatl genes	1.593
4	L12168	*CAP1*	Adenylyl cyclase-associated protein 1	1.588
5	M21121	*CCL5*	Chemokine (C-C motif) ligand 5	1.581
6	U68727	*PKNOX1*	PBX/knotted 1 homeobox 1	1.507
7	U45878	*BIRC3*	Baculoviral IAP repeat-containing 3, API2	1.489
8	M19720	*MYCL1*	Human L-myc oncogene	1.482
9	HG2639-HT2735	*RBMS1*	Single stranded interacting protein 1	1.439
10	M12529	*APOE*	Apolipoprotein E	1.413
11	HG1437-HT1437	*TPM4*	Tropomyosin 4, TRKA	1.404
12	J05008	*IL1B*	Homo sapiens endothelin-1	1.392
13	J03805	*PPP2CB*	Protein phosphatase 2, catalytic subunit	1.361
14	M98539	*PTGDS*	Human prostaglandin D2 synthase gene	1.360
15	U40343	*CDKN2D*	Cyclin-dependent kinase inhibitor 2D	1.354
16	U66406	*EFNB3*	Putative EPH-related PTK receptor ligand	1.314
17	L06139	*TEK*	Tyrosine kinase, endothelial	1.313
18	L07594	*TGFBR3*	Transforming growth factor–β type receptor III	1.308
19	M59465	*TNFAIP3*	Tumor necrosis factor α inducible protein 3	1.291
20	M65290	*IL12B*	Interleukin 12B	1.277
21	HG2463-HT2559	*CDC42*	Guanine nucleotide-binding protein	1.271
22	U53446	*DOC-2*	Mitogen-responsive phosphoprotein	1.256
23	M26683	*CCL2*	Interferon gamma treatment inducible	1.250
24	L36870	*MKK4*	Mrna Homo sapiens MAP kinase 4	1.248
25	HG2774-HT2820	*CDC42*	Cell division cycle 42	1.241
26	M34668	*PTPRA*	Protein tyrosine phosphatase, receptor type A	1.226
27	S76965	*PKIA*	Protein kinase inhibitor α	1.218
28	M65254	*PPP2R1B*	Phosphatase 2, regulatory subunit A, β isoform	1.192
29	U67156	*MAP3K5*	Mitogen-activated protein kinase kinase kinase 5	1.174
30	U57650	*INPP5D*	Inositol polyphosphate-5-phosphatase, 145Da	1.168

S/N value reflects the difference between early and advanced stage of the patients. The genes examined by real-time PCR are indicated by underlining.

crease in aggressive NB (Leone et al., 1993; Godfriend et al., 2002), was also assigned to the group containing the most highly expressed genes in advanced-stage tumors. *MYCN* amplification was detected in 3 of the 20 cases. Using microarray analysis, high expression of *MYCN* was detected in those 3 cases and in an additional 2 cases without *MYCN* amplification. *MYCN* expression was considered high if the expression ratio was less than 2 SD from the mean in 20 cases according to microarray analysis.

Semiquantitative RT-PCR Analysis

To validate the results of the microarray analysis, we performed a semiquantitative RT-PCR analysis of 6 known genes, which were selected because of their typical expression in each cluster. The S/N value of each gene, reflecting the difference between the early- and advanced-stage tumors, was greater than 1 (Mukasa et al., 2002). The same 20 samples used for microarray analysis were used for the RT-PCR analysis, and representative results are shown in Figure 3. The signal intensity of the 6 genes' expression by RT-PCR was calculated and classified (+ and −) with a scanning densitometer and data analysis system (Discovery Series; Quantity One, PDI). A highly abundant expression level (+) was above average and a reduced expression level (−) below average. As shown in Figure 3, the microarray intensity score of the 6 genes and the results of RT-PCR analysis corresponded well, indicating that the array-based determinations were highly reproducible.

PCA Analysis

Principal-components analysis also was used for further investigation of the structure of the data. A PCA three-dimensional plot of all the specimens used for the microarray analysis is shown in Figure 4. As can be seen, the tumors examined were clearly separated by the stage-of-disease subgroups (Fig. 4). From this analysis, it can be seen that classification by stage-of-disease subgroups resulted in clearer differentiation than classification

TABLE 4. Genes Showing Higher Expression in Advanced-Stage Tumors

No.	Accession number	Symbol	Description	S/N value
1	M87339	*RFC4*	Human replication factor C	−2.112
2	L76191	*IRAK1*	Interleukin-1 receptor-associated kinase 1	−1.801
3	U66619	*SMARCD3*	SWI/SNF related, subfamily d, member 3	−1.733
4	M91670	*UBE2S*	Ubiquitin-conjugating enzyme E2S	−1.677
5	D64142	*H1FX*	Histone family, member X	−1.652
6	U37689	*POLR2H*	Polymerase (RNA) II polypeptide H	−1.519
7	M27830	*RNR1*	Human 28S ribosomal RNA gene	−1.442
8	Z97074	*RAB9P40*	Rab9 effector p40	−1.433
9	HG960-HT960	*SOS*	Son of sevenless homolog 1 (Drosophila)	−1.348
10	L24559	*POLA2*	Polymerase (DNA-directed), alpha (70kD)	−1.309
11	U65402	*GPR31*	Seven transmembrane G-couples receptor	−1.295
12	X73066	*NME1*	Non-metastatic cells 1, NM23-H1	−1.287
13	L19686	*MIF*	Macrophage migration inhibitor factor	−1.277
14	HG3729-HT3999	*HSHPX5*	Homeotic protein Hpx-5	−1.207
15	D78586	*CAD*	Carbamoyl-phosphate synthetase 2	−1.205
16	D14678	*KIFC1*	Kinesin family member C1	−1.171
17	HG4074-HT4344	*FEN1*	Flap structure-specific endonuclease 1	−1.167
18	U90426	*DDX5*	Nuclear RNA helicase	−1.166
19	D14889	*DDX39*	DEAD (Asp-Glu-Ala-Asp) box polypeptide 39	−1.161
20	U73379	*UBE2C*	Ubiquitin-conjugating enzyme E2C	−1.159
21	X74795	*MCM5*	Minichromosome maintenance deficient 5	−1.157
22	U64871	*LTB4R*	Gprotein-coupled receptor	−1.152
23	U14394	*TIMP3*	Tissue inhibitor of metalloproteinase 3	−1.101
24	U76638	*BARD1*	BRCA1 associated RING domain 1	−1.091
25	D55716	*MCM7*	Minichromosome maintenance deficient 7	−1.063
26	HG919-HT919	*POLEDNA*	Polymerase (DNA directed), epsilon	−1.054
27	S69370	*PAX3B*	Transcription factor	−1.051
28	L25876	*CDKN3*	Cyclin-dependent kinase inhibitor 3	−1.017
29	M13228	*MYCN*	Human N-myc oncogene	−1.007
30	U07664	*HB9*	Human HB9 homeobox gene	−1.001

S/N value reflects the difference between early and advanced stages of the patients. The genes examined by real-time PCR are indicated by underlining.

by two-way clustering analysis. Supplementary data are available at http://www2.genome.rcast.u-tokyo.ac.jp/NBL/supp.html.

Relationship between Clinicopathological Findings and Expression of *API2*, *p19INK4D*, and *BAF60c* Genes in NB

Because the functions of the *BIRC3*, *CDKN2D*, and *SMARCD3* genes are known to be related to apoptosis, the cell cycle, and transcriptional activation, respectively (Guan et al., 1996; Wang et al., 1996; LaCasse et al., 1998), it is possible that these genes are involved in the progression of NB. Thus, to clarify the biological significance of the expression of these genes in NB, we did additional quantitative real-time PCR analysis on a total of 50 NB samples. The *TRKA* and *NME1* genes were excluded from this study because they are already known as prognostic factors in NB (Leone et al., 1993; Nakagawara et al., 1993; Godfriend et al., 2002). Normal adrenal gland tissue (Clontech) was used as the control, and target gene expression was normalized to that of *β-actin*. The expression of the *BIRC3* gene was significantly higher in stage-1 and -2 patients than in stage-4 patients ($P = 0.002$ and 0.001; Fig. 5A). Furthermore, significantly higher expression of the *BIRC3* gene was observed in the tumors detected by our mass screening program than in those detected by the clinical course ($P = 0.031$). *BIRC3* expression was also significantly higher in the patients under 1 year of age than in those more than 1 year old ($P = 0.021$). Much higher expression of the *BIRC3* gene was detected in only 1 of 4 tumors with *MYCN* amplification, and the average expression level of the *BIRC3* gene in the tumor with *MYCN* amplification was low. *BIRC3* expression in the normal adrenal gland was as low as in the tumors of stage-4 and -4S patients (Fig. 5A).

The expression of the *CDKN2D* gene was significantly higher in stage-1 and -2 patients than in stage-4 patients ($P = 0.012$ and 0.009; Fig. 5C). Expression of *CDKN2D* just as significantly high was observed in both groups detected by the mass screening program and in infants ($P = 0.04$). Ex-

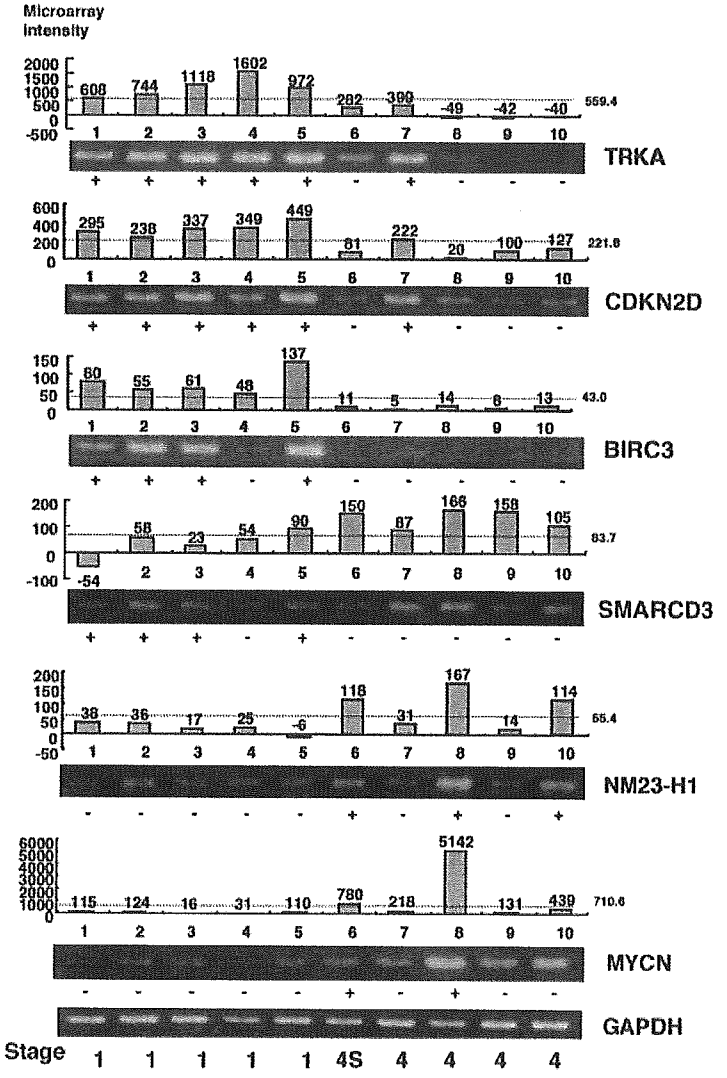

Figure 3. Semiquantitative RT-PCR analysis. Representative results for 10 of the 20 samples examined are shown in this figure. The upper three genes are those that showed higher expression in early-stage tumors, and the lower three genes those that showed higher expression in advanced-stage tumors. GAPDH was used as a control. The microarray intensity score of each gene also is indicated. The mean microarray intensity score of each gene is indicated as a dotted line.

tremely low *CDKN2D* expression was found in tumors with *MYCN* amplification. The *CDKN2D* expression in the normal adrenal gland was higher than in the tumors of stage-4 and -4S patients (Fig. 5C).

SMARCD3 expression was significantly higher in stage-4 patients than in stage-1 and -2 patients ($P = 0.03$ and 0.038, respectively). Although the tumor of the stage-4S patient had a tendency to higher *SMARCD3* expression than that of stage-1 and -2 patients, no significant difference was observed. High expression of the *SMARCD3* gene was detected in all patients with *MYCN* amplification. *SMARCD3* expression in the normal adrenal gland was as low as in the tumors of stage-1, -2, and -3 patients (Fig. 5 D). To investigate the correlation between the expression of the genes as measured by microarray and by real-time PCR analyses, we compared the intensity score of *BIRC3* determined by microarray and real-time PCR analyses in 20 samples (Fig. 6). As shown in Figure 6, the coefficient was as high as 0.968 ($n = 20$, $P < 0.0001$), indicating that the expression intensity of *BIRC3* detected by microarray analysis corresponded well to that detected by real-time PCR analysis.

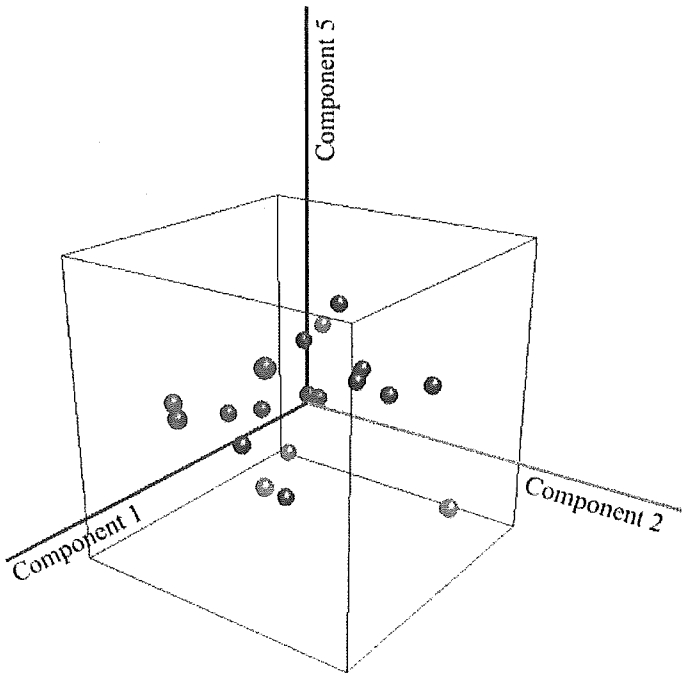

Figure 4. PCA three-dimensional plot of the 20 samples. Stage-of-disease subgroups (stages 1, 2, 4S, and 4) are indicated. Blue plots represent tumors classified as stage 1, green plots those classified as stage 2, red plots those classified as stage 4, and pink plots those classified as stage 4S.

Expression of *BIRC3*, *CDKN2D*, and *SMARCD3* Genes in NB Cell Lines

We also analyzed the expression patterns of the *BIRC3*, *CDKN2D*, and *SMARCD3* genes in 27 NB cell lines with real-time PCR analysis. The expression of these three genes was detected in all 27 cell lines. Significantly lower expression of both the *BIRC3* and *CDKN2D* genes was observed in the cell lines than in the primary tumors of NB (P = 0.002 and 0.003, respectively), whereas expression of the *SMARCD3* gene was significantly higher in the cell lines than in the primary NB tumors (P = 0.001).

Expression of *BIRC2*, *SMARCD1*, and *SMARCD2* Genes in NB

The *BIRC3* gene has a high homology to the *BIRC2* gene, and these two genes sit in tandem on chromosome band 11q21, with an intergenic distance of approximately 7 kb (Young et al., 1999). The tissue distributions and functions of the *BIRC2* and *BIRC3* genes appear to be similar, although the relative expression of the *BIRC3* is generally higher (Young et al., 1999). Moreover, the *SMARCD3* gene has two homologs, *SMARCD1* and *SMARCD2*, and they share 70%–80% identity with each other (Wang et al., 1996). Thus, to determine whether the *BIRC2*, *SMARCD1*, and *SMARCD2* genes could be additional prognostic markers for NB, we further examined these gene expression patterns in 50 primary tumors and 27 cell lines of NB by real-time RT-PCR analysis. Generally, low expression levels of the *BIRC2* gene were detected in the adrenal gland, primary tumors, and cell lines of NB, indicating obvious differences in expression patterns between *BIRC2* and *BIRC3* in NB (Fig. 5A and B). Despite the extremely high expressions of *SMARCD1* and *SMARCD2* in the cell lines, both genes showed low expression in the primary tumors. No significantly different expression patterns of these genes between the early and advanced stages of NB were observed (Fig. 5E and F).

DISCUSSION

We have shown the global gene expression profiles of NB and that we were able to identify genes that are differentially expressed between the early and advanced stages of NB. The results of RT-PCR analysis of the several identified genes were concordant with the microarray analysis data, confirming the fidelity of the system. By two-way clustering analysis, the 20 NB samples were classified into two main phylogenic groups, indicating the existence of at least two major genetic subgroups in